International Journal of Heat and Mass Transfer 135 (2019) 1118–1129

Contents lists available at ScienceDirect

International Journal of Heat and Mass Transfer

journal homepage: www.elsevier.com/locate/ijhmt

Scaling expressions of characteristic values for a moving point heat source in steady state on a semi-infinite solid

Ying Wang [a], Yi Lu [a,*], Patricio F. Mendez [b]

[a] Chemical and Materials Engineering, University of Alberta, Canada
[b] Chemical and Materials Engineering, University of Alberta, Donadeo ICE 12-332, 9211 116St, Edmonton, AB T6G 2V4, Canada

ARTICLE INFO

Article history:
Received 16 October 2018
Received in revised form 9 February 2019
Accepted 12 February 2019

Keywords:
Analytical modeling
Heat conduction
Scaling analysis

ABSTRACT

Engineering expressions for characteristic values of a moving point heat source on a semi-infinite solid are presented. Related characteristic values are: maximum isotherm width and its location, leading and trailing lengths of isotherm, centerline heating rate and cooling rate, maximum temperature and its gradient at maximum width, aspect ratio of isotherms, melting efficiency, cooling time from 800 °C to 500 °C (often used for studying steels), solidification time, the thickness of zone affected by the heat source, and modification criteria to account for the effect of joint preparation. All engineering expressions proposed are accurate to within 7% of the exact analytical solutions, and are obtained with a systematic approach. Dimensional analysis indicates that the expressions developed depend on a single dimensionless parameter that captures all possible cases. This dimensionless number is typically the Rykalin number (Ry), which characterizes three dimensional heat flow induced by a moving point heat source. The obtained engineering equations are of great practical value for very diverse fields where moving heat sources are involved, and are simple enough to be calculated with a calculator or spreadsheet.

© 2019 Published by Elsevier Ltd.

1. Introduction

This paper applies the methodology of scaling analysis, asymptotic analysis, and correction factors based on blending techniques to the calculation of 13 technologically relevant characteristic values of moving point heat sources (represented in Fig. 1) associated with the isotherm $T(x,y,z) = T_c$. The method of analysis is explained in detail in [1] where the maximum isotherm width and its location (y_{max} and x_{max}) were analyzed as demonstration examples. This paper focuses on 6 new primary characteristic values, and 5 secondary characteristic values associated with the primary ones. The primary characteristic values studied are: the trailing length of isotherm x_b, the leading length of isotherm x_f, the centerline cooling rate $\dot{T}_b$, the centerline heating rate $\dot{T}_f$, the maximum temperature of a point in the cross section T_{max} and the transverse temperature gradient at the maximum isotherm width dT_{max}/dy. The secondary characteristic values are the aspect ratio A_R of the chosen isotherm (indicating how elongated it is), the melting efficiency η_m (in this case as a rough approximation useful to estimate the dilution of filler metal in welding), cooling time from 800 °C to 500 °C ($t_{8/5}$, a standard metric of rate of cooling in the welding of steels), solidification time t_{sl}, (the time interval for the base material to solidify over a range of temperature) and the separation between the maximum width of two isotherms Δy_{HAZ} (useful to assess thickness of the heat affected zone in welding). The cylindrical symmetry of the idealized problem formulation also enables the generalization of results to other geometries with cylindrical symmetry, such as edges, corners, and bevels.

The methodology employed here is based on the solution for a moving point heat source in quasi-stationary state on a semi-infinite solid presented in [2–4], and typically called "Rosenthal solution"

$$T(x,y,z) = T_0 + \frac{q}{2\pi kr}\exp\left[-\frac{U}{2\alpha}(r+x)\right] \quad (1)$$

where x, y, and z are the independent variables illustrated in Fig. 1, q is the intensity of the point heat source, k is the thermal conductivity of the substrate, T_0 is the temperature of the substrate far from the heat source, U is the velocity of the heat source relative to the substrate, and α is the thermal diffusivity of the substrate. The radial coordinate r is defined in relation to the independent variables as $r = \sqrt{x^2+y^2+z^2}$. Eq. (1) can be rewritten in normalized form as

* Corresponding author.
E-mail addresses: wang18@ualberta.ca (Y. Wang), ylu13@ualberta.ca (Y. Lu), pmendez@ualberta.ca (P.F. Mendez).

https://doi.org/10.1016/j.ijheatmasstransfer.2019.02.042
0017-9310/© 2019 Published by Elsevier Ltd.

Notation

Variable	Description (Unit)
A_R	aspect ratio of isotherm (1)
c_p	specific heat (J kg^{-1} K^{-1})
k	thermal conductivity (W m^{-1} K^{-1})
q	power of heat source absorbed by substrate (W)
r	distance from the heat source (m)
Ry	Rykalin number (1)
St	Stefan number (1)
t	time (s)
t_{sl}	solidification time at centerline (s)
$t_{8/5}$	cooling time from 800 °C to 500 °C (s)
T	temperature (K)
T_0	initial temperature (K)
T_c	temperature of interest (K)
T_{HAZ}	temperature of edge of HAZ (K)
T_{max}	maximum temperature (K)
$\dot{T}_b$	centerline cooling rate (K s^{-1})
$\dot{T}_f$	centerline heating rate (K s^{-1})
dT_{max}/dy	gradient of maximum temperature (K m^{-1})
U	travel speed of moving heat source (m s^{-1})
W_0	Lambert function (–)
x, y, z	Cartesian coordinates (m)
x_b	trailing length of isotherm (m)
x_f	leading length of isotherm (m)
x_{max}	location of maximum isotherm width (m)
y_{max}	maximum isotherm width (m)
Δy_{HAZ}	thickness of the affected zone (m)

Greek symbols

α	thermal diffusivity (m^2 s^{-1})
η_m	melting efficiency (1)
ϕ	actual heat flow angle (°)
ρ	density (kg m^{-3})

Superscripts

*	dimensionless value
$\widehat{\ }$	asymptotic behavior
$^+$	correction for intermediate values
$\dot{\ }$ symbol	time derivative

Subscripts

I	corresponding to Regime I
II	corresponding to Regime II

$$T^* = \frac{1}{r^*}\exp\left(-r^* - x^*\right) \tag{2}$$

where

$$T^* = \frac{4\pi k\alpha(T - T_0)}{qU} \tag{3}$$

$$x^* = \frac{Ux}{2\alpha} \tag{4}$$

$$y^* = \frac{Uy}{2\alpha} \tag{5}$$

$$z^* = \frac{Uz}{2\alpha} \tag{6}$$

$$r^* = \frac{Ur}{2\alpha} \tag{7}$$

In Eqs. (3)–(7) the * superscript indicates a dimensionless quantity. Dimensional analysis indicates that for a selected isotherm $T = T_c$, all dimensionless characteristic values depend only on the Rykalin number (Ry) proposed by Fuerschbach [5,1]

$$\mathrm{Ry} = \frac{qU}{4\pi k\alpha(T_c - T_0)} \tag{8}$$

The Rykalin number is the reciprocal of T^* for $T = T_c$, and can be interpreted as a Peclet number ($\mathrm{Pe} = U\mathcal{L}/\alpha$) where the characteristic length $\mathcal{L}$ is related to the gradient induced by the heat source: $\mathcal{L} = q/[4\pi k(T_c - T_0)]$. The Peclet number relates the effect of advection relative to conduction and therefore a high Ry value can be interpreted as a "fast heat source" where advection dominates over conduction, and a low Ry value can be interpreted as a "slow heat source" with heat transfer dominated by conduction. The use of Churchill-Usagi blending techniques [6,7] to estimate intermediate values based on the limiting cases was pioneered in [8].

In the following sections, closed-form expressions of characteristic values in high and low Ry asymptotic regimes are presented, and blending functions are used to provide estimates at the intermediate regime with high accuracy and simplicity. The blending then becomes the basis of correction factors suitable for engineering applications. Finally, engineering expressions suitable for use by practitioners are presented.

2. Maximum isotherm width y_{max} and its location x_{max}

The maximum isotherm width is a parameter of much practical value, since it can be measured from cross sections of samples. Temperatures of relevance include the melting temperature (for the case of welding) and the austenitization temperature (for the case of moving heat sources on steel). Explicit estimates and associated correction factors were derived in [1]. For maximum isotherm width, the asymptotic behavior in dimensionless form is

$$\widehat{y^*}_{\max_I}(\mathrm{Ry}) = \sqrt{\frac{2\mathrm{Ry}}{\mathrm{e}}} \quad \text{for Regime I (fast)} \tag{9}$$

$$\widehat{y^*}_{\max_{II}}(\mathrm{Ry}) = \mathrm{Ry} \quad \text{for Regime II (slow)} \tag{10}$$

and the corresponding practical engineering expressions with correction factors are

$$\hat{y}^+_{\max} = \hat{y}_{\max_I} f_{y_{\max_I}}(\mathrm{Ry}) = \sqrt{\frac{2}{\pi\mathrm{e}}\frac{\alpha q}{Uk(T_c - T_0)}}\, f_{y_{\max_I}}(\mathrm{Ry}) \quad \text{for Regime I (fast)} \tag{11}$$

$$\hat{y}^+_{\max} = \hat{y}_{\max_{II}} f_{y_{\max_{II}}}(\mathrm{Ry}) = \frac{1}{2\pi}\frac{q}{k(T_c - T_0)}\, f_{y_{\max_{II}}}(\mathrm{Ry}) \quad \text{for Regime II (slow)} \tag{12}$$

$$f_{y_{\max_{I,II}}}(\mathrm{Ry}) = \left[1 + \left(\sqrt{\mathrm{eRy}/2}\right)^{\pm n}\right]^{1/n} \quad n = -1.731 \tag{13}$$

where the value of the exponent n was determined through the optimization process described in [1]. The functional form of Eq. (13) was proposed originally by Acrivos [9,10] and further developed by Churchill and Usagi [6,7]. The most important features of this blending approach are that it matches exactly the asymptotic behavior for large and small values (in this case, values of Ry), making it rigorous and general; it has a single fitting parameter, making it computationally efficient; and typically yields approximations within a few percentage points of the exact solution over the whole domain, making it credible and useful in practice.

For the location of maximum isotherm width, the asymptotic behavior in dimensionless form is

$$\widehat{x}^{*}_{\max_{\mathrm{I}}}(\mathrm{Ry}) = -\frac{\mathrm{Ry}}{\mathrm{e}} \quad \text{for Regime I (fast)} \tag{14}$$

$$\widehat{x}^{*}_{\max_{\mathrm{II}}}(\mathrm{Ry}) = -\mathrm{Ry}^{2} \quad \text{for Regime II (slow)} \tag{15}$$

resulting in the following practical engineering expressions

$$\widehat{x}^{+}_{\max} = \widehat{x}_{\max_{\mathrm{I}}} f_{x_{\max_{\mathrm{I}}}}(\mathrm{Ry}) = -\frac{q}{2\pi \mathrm{e} k(T_{\mathrm{c}} - T_0)} f_{x_{\max_{\mathrm{I}}}}(\mathrm{Ry}) \quad \text{for Regime I (fast)} \tag{16}$$

$$\widehat{x}^{+}_{\max} = \widehat{x}_{\max_{\mathrm{II}}} f_{x_{\max_{\mathrm{II}}}}(\mathrm{Ry}) = -\frac{2U}{\alpha}\left[\frac{q}{4\pi k(T_{\mathrm{c}} - T_0)}\right]^{2} f_{x_{\max_{\mathrm{II}}}}(\mathrm{Ry}) \quad \text{for Regime II (slow)} \tag{17}$$

$$f_{x_{\max_{\mathrm{I,II}}}}(\mathrm{Ry}) = \left[1 + (\mathrm{eRy})^{\pm n}\right]^{1/n} \quad n = -0.9990 \tag{18}$$

In Eqs. (13) and (18), the positive sign corresponds to Regime I ($f_{y_{\max_{\mathrm{I}}}}, f_{x_{\max_{\mathrm{I}}}}$), and the negative sign corresponds to Regime II ($f_{y_{\max_{\mathrm{II}}}}, f_{x_{\max_{\mathrm{II}}}}$).

3. Trailing length of isotherm x_{b}

The trailing length of an isotherm, x_{b}, is the length of the "hot tail" trailing the heat source. In the case of welding, the trailing length of the isotherm of melting temperature estimates the length of the molten tail (which is often protected with inert gases of limited reach). The trailing length, together with the maximum isotherm width are geometrical parameters often used to characterize the shape of the melt pool in welding and laser cladding [11,12], and has been used as a variable in electron beam manufacturing (EBM) processes [13,14]. For the problem formulation captured by Eq. (2), x^{*}_{b} is calculated by solving the equation at the centerline ($y^{*} = 0, z^{*} = 0$), and $T = T_{\mathrm{c}}$. This equation has two roots; x^{*}_{b} is the negative root, while the positive root is x^{*}_{f}, which will be discussed later. For both roots, the exact solution is in closed form, and covers the whole range of Ry from Regime I ($\mathrm{Ry} \to \infty$) through Regime II ($\mathrm{Ry} \to 0$); therefore, asymptotic approximations and blending are not necessary. In dimensionless form, the expression of x^{*}_{b} is

$$x^{*}_{\mathrm{b}}(\mathrm{Ry}) = -\mathrm{Ry} \quad \text{Regime I (fast) and II (slow)} \tag{19}$$

where the $\widehat{\ }$ symbol is not used because the above equation is an exact expression, not an asymptotic approximation. The corresponding engineering expression with units is obtained by replacing Eqs. (4) and (8) into Eq. (19), obtaining

$$x_{\mathrm{b}} = -\frac{q}{2\pi k(T_{\mathrm{c}} - T_0)} \quad \text{Regime I (fast) and II (slow)} \tag{20}$$

4. Centerline cooling rate $\dot{T}_{\mathrm{b}}$

The centerline cooling rate, $\dot{T}_{\mathrm{b}}$, evaluated at temperature T_{c}, is one of the most important characteristic values associated with

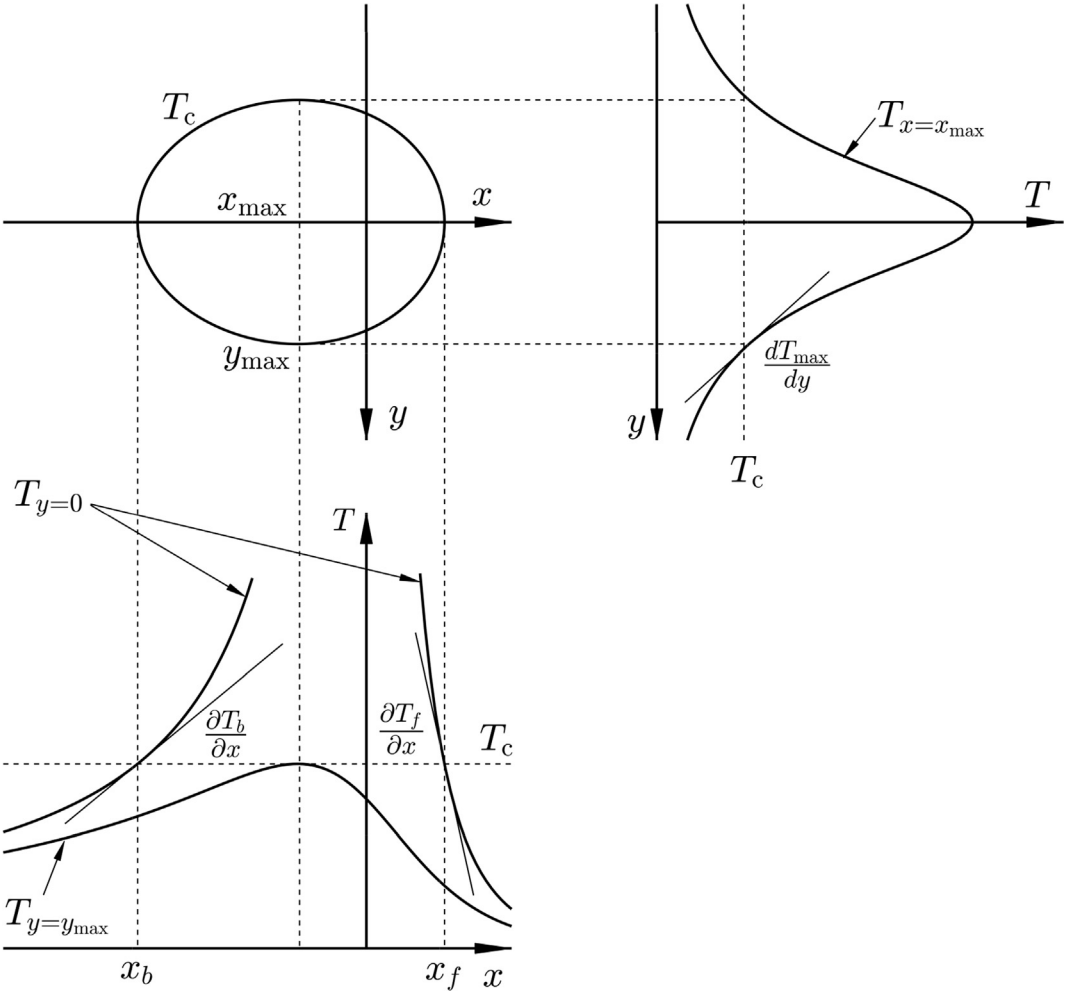

Fig. 1. Characteristic values of isotherm $T = T_{\mathrm{c}}$ for a moving point heat source on a semi-infinite solid.

moving heat sources, and in most practical cases, the centerline cooling rate is representative of the cooling rate of the whole area affected by the heat source [15,16]. The centerline cooling rate is crucial to determine the microstructure and mechanical properties such as hardness and strength in metals. For example, for the case of steels, for a given composition and austenite grain size, their hardness is almost completely determined by the cooling rate at a temperature near the transformation temperature (approximately 700 °C) [17,18].

To calculate the rate of temperature variation at a particular point in the substrate (which is moving relative to the heat source), the concept of material derivative is needed

$$\frac{DT}{Dt} = \frac{\partial T}{\partial t} - U\frac{\partial T}{\partial x} \tag{21}$$

where $\partial T/\partial t = 0$ in the pseudo-steady state of the problem formulation. Eq. (21), together with Eqs. (3) and (4) yield the following normalization for time t

$$t^* = \frac{U^2 t}{2\alpha} \tag{22}$$

resulting in

$$\frac{DT^*}{Dt^*} = -\frac{\partial T^*}{\partial x^*} \tag{23}$$

The derivative $\partial T^*/\partial x^*$ at the centerline is directly derived from Eq. (2). Similarly to the case of x_b, an exact closed-form solution covers the whole range of Ry and neither asymptotic approximations nor blending are necessary. In dimensionless form

$$\left.\frac{DT^*}{Dt^*}\right|_b (\mathrm{Ry}) = -\mathrm{Ry}^{-2} \quad \text{Regime I (fast) and II (slow)} \tag{24}$$

The corresponding engineering expression with units can be obtained by replacing Eqs. (3), (8) and (22) into Eq. (24)

$$\dot{T}_b = -\frac{2\pi k U (T_c - T_0)^2}{q} \quad \text{Regime I (fast) and II (slow)} \tag{25}$$

Eq. (25) is identical to the expressions presented in [19,16], and it has been widely used in practice in applications such as welding [20], laser processing [21,22], and many other more. Empirical approximations based on modifications of this formula have been proposed in [23–26]; for example, a modification of the exponent of temperature difference as follows [23,25]

$$\dot{T}_b \propto (T_c - T_0)^n \tag{26}$$

where the proposed value of n for the welding of steels is approximately 1.8, very close to the theoretical value of 2. This modified exponent captures in a rough form the physical effects beyond the limitations of Rosenthal's model (finite heat source, latent heat, non-insulated surface, convection in the melt, etc.). It is remarkable that the extremely idealized Rosenthal model yields a dependence on temperature so close to what is seen in practice.

5. Leading length of isotherm x_f

The leading length of an isotherm, x_f, is an indication of how far the heat travels by conduction (and against advection) ahead of the heat source. If the melting isotherm is considered, x_f is a metric of how much the molten bead "leads" the heat source. The leading length is of much technological relevance in welding, laser cladding, and additive manufacturing [27,28].

As mentioned in the discussion of x_b^*, x_f^* involves solving Eq. (2) for $T = T_c$ at the centerline, but in this case, using the positive root. The exact solution can be expressed in a simple form using the Lambert W_0 function and covers the whole range of Ry; therefore, no blending or correction functions are necessary.

$$x_f^*(\mathrm{Ry}) = \frac{1}{2}W_0(2\mathrm{Ry}) \quad \text{Regime I (fast) and II (slow)} \tag{27}$$

where $W_0(\xi)$ is the positive branch of the solution of the equation $\xi = W\exp(W)$ [29] as shown in Fig. 2.

The Lambert function is implemented into common scientific software such as Matlab, Maple, Mathematica, and online calculation tools such as WolframAlpha. Although the Lambert function is non-elementary, it can be approximated using elementary functions (28) [30] as shown below

$$\widehat{W}_0(x) \approx (1+\epsilon)\ln\left\{\frac{1.2x}{\ln\left[\frac{2.4x}{\ln(1+2.4x)}\right]}\right\} - \epsilon\ln\left[\frac{2x}{\ln(1+2x)}\right] \tag{28}$$

where $\epsilon \approx 0.46$, and the relative error is below $2\ 10^{-3}$.

The dimensional engineering expression for leading length can be obtained by replacing Eq. (4) into Eq. (27), obtaining

$$x_f = \frac{\alpha}{U}W_0\left[\frac{qU}{2\pi k\alpha(T_c - T_0)}\right] \quad \text{Regime I (fast) and II (slow)} \tag{29}$$

6. Centerline heating rate $\dot{T}_f$

The centerline heating rate ahead of the heat source, $\dot{T}_f$, is relevant to understand phase transformations in thermal processes. For example, during heating, steels experience a phase transformation from ferrite to austenite around 700 °C (The temperature at which the transformation starts depends on the alloy, and it is called $A_{c,1}$, and the temperature at which the transformation is complete $A_{c,3}$). Both temperatures are significantly affected by the heating rate, and in the ignorance of the rate of heating, these temperatures are assumed to be those measured in near-equilibrium conditions, resulting in predictions of transformed region larger than seen in reality. Another example of relevance of the heating rate is the case of welding of Zn-coated steels. The Zn coating tends to evaporate ahead of the weld, preventing porosity in the weld; however, if the rate of heating is faster than the rate of evaporation, Zn might remain on the surface and become entrapped in the melt, causing porosity.

The centerline heating rate $\dot{T}_f$ shares the same derivation process as centerline cooling rate $\dot{T}_b$. The temperature evolution at the leading length of an isotherm when the heat source approaches is also captured by Eq. (23). The exact solution can be calculated in exact form using the first derivative of Lambert W function [29], and it covers the whole range of Ry, so neither asymptotic approximations nor blending are necessary. In dimensionless form, the expression of DT^*/Dt^* is

$$\left.\frac{DT^*}{Dt^*}\right|_f = \frac{2}{\mathrm{Ry}}\left[\frac{1}{W_0(2\mathrm{Ry})} + 1\right] \quad \text{Regime I (fast) and II (slow)} \tag{30}$$

The corresponding engineering expression with units can be obtained by replacing Eqs. (3), (8), and (22) into Eq. (30)

$$\dot{T}_f = \frac{U^2(T_c - T_0)}{\alpha}\left[\frac{1}{W_0(2\mathrm{Ry})} + 1\right] \quad \text{Regime I (fast) and II (slow)} \tag{31}$$

7. Maximum temperature T_{max}

The maximum temperature reached at a given point in a cross section gives an indication of possible phase changes, phase

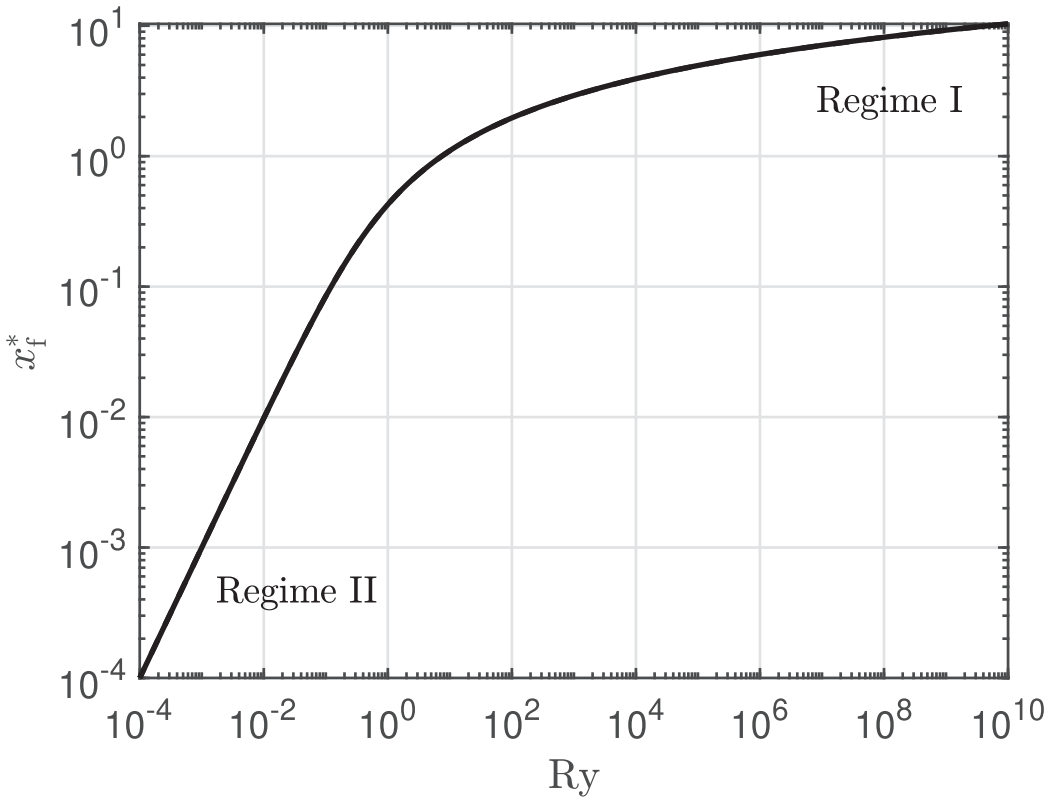

Fig. 2. Dimensionless leading length as a function of Ry. The exact solution and the approximation of Eq. (28) overlap within the thickness of the line.

transformations, thermodynamic effects, or practical defects that might happen. With the cylindrical symmetry of the formulation used, any point on the cross section is equivalent to a point on the surface ($z^* = 0$) at the same radial distance from the centerline $y^* = y_c^*$. In this case, the target characteristic value T_{max}^* depends only on the dimensionless group y_c^*, rather than Ry as in the previous cases. The reason is that dimensionless temperature T^* and Ry are directly related by $T_c^* = 1/\mathrm{Ry}$; therefore, this case can be interpreted as the reverse of the calculation of $y_{max}^*(\mathrm{Ry})$ studied in [1]. The location of the maximum temperature at $y^* = y_c^*$ is $x^* = x_{max}^*$, such that $x_{max}^* = x_{max}^*(y_c^*)$. This way, $\max[T^*(x^*, y_c^*, 0)] = T^*(x_{max}^*, y_c^*, 0) = T_{max}^*(y_c^*)$. Asymptotic analysis of Eq. (2) yields the following power laws for Regime I (fast) and Regime II (slow)

$$\widehat{T^*}_{\max_I}(y_c^*) = \frac{2}{\mathrm{e}y_c^{*2}} \quad \text{for Regime I (fast)} \tag{32}$$

$$\widehat{T^*}_{\max_{II}}(y_c^*) = \frac{1}{y_c^*} \quad \text{for Regime II (slow)} \tag{33}$$

Eq. (32) is in agreement with the expression derived by Adams in [16] for fast welds. Adams expression, despite an apparent attempt at blending, breaks down for slow welds. The blending techniques detailed in [1] result in the following correction factors

$$f_{T_{\max_{I,II}}}(y_c^*) = \left[1 + \left(\frac{\mathrm{e}y_c^*}{2}\right)^{\pm n}\right]^{1/n} \qquad \begin{matrix} +n \text{ for Regime I (fast)} \\ -n \text{ for Regime II (slow)} \end{matrix} \tag{34}$$

The optimal value of n for Eq. (34) is $n = -1.246$, with an error always less than 3.880%. The crossover point for the correction factors is $y_c^* = 0.7363$. Asymptotic expressions without correction factors result in an error less than 10% for $y_{c_I}^* > 2.809$ or $y_{c_{II}}^* < 0.1050$ in their corresponding regimes.

The corresponding engineering expression with units can be obtained by replacing Eq. (8) into Eqs. (32) and (33) and combining with Eq. (3)

$$\widehat{T}_{max}^{+} = \widehat{T}_{\max_I} f_{T_{\max_I}}(y_c^*) = T_0 + \frac{2\alpha q}{\mathrm{e}\pi k U y_c^2} f_{T_{\max_I}}(y_c^*) \quad \text{for Regime I (fast)} \tag{35}$$

$$\widehat{T}_{max}^{+} = \widehat{T}_{\max_{II}} f_{T_{\max_{II}}}(y_c^*) = T_0 + \frac{q}{2\pi k y_c} f_{T_{\max_{II}}}(y_c^*) \quad \text{for Regime II (slow)} \tag{36}$$

8. Gradient of maximum temperature dT_{max}/dy

The gradient of maximum temperature is a useful intermediate step to approximate the distance between two important temperatures that can be identified in a cross section, for example, this gradient can be used to estimate the thickness of the heat affected zone (HAZ) in welding. Because the HAZ is typically thin, the error of using the gradient instead of the exact subtraction is typically negligible. The advantage of using the gradient instead of subtracting the maximum widths corresponding to the two target temperatures is that the gradient yields a power-law answer, which is convenient to see intuitively the interplay of parameters.

The dimensionless form of the gradient of maximum temperature can be analyzed by expanding the derivative of $T_{max}^* = T(x_{max}^*(y^*), y^*, 0)$, and evaluating it at point $(x_{max}^*, y_c^*, 0)$

$$\frac{dT_{max}^*}{dy^*} = \frac{\partial T^*}{\partial x^*}\frac{dx_{max}^*}{dy^*} + \frac{\partial T^*}{\partial y^*} \tag{37}$$

where $\partial T^*/\partial x^* = 0$ at $x = x_{max}^*$, by definition; therefore $dT_{max}^*/dy^* = dT^*/dy^*$ yielding the following power laws

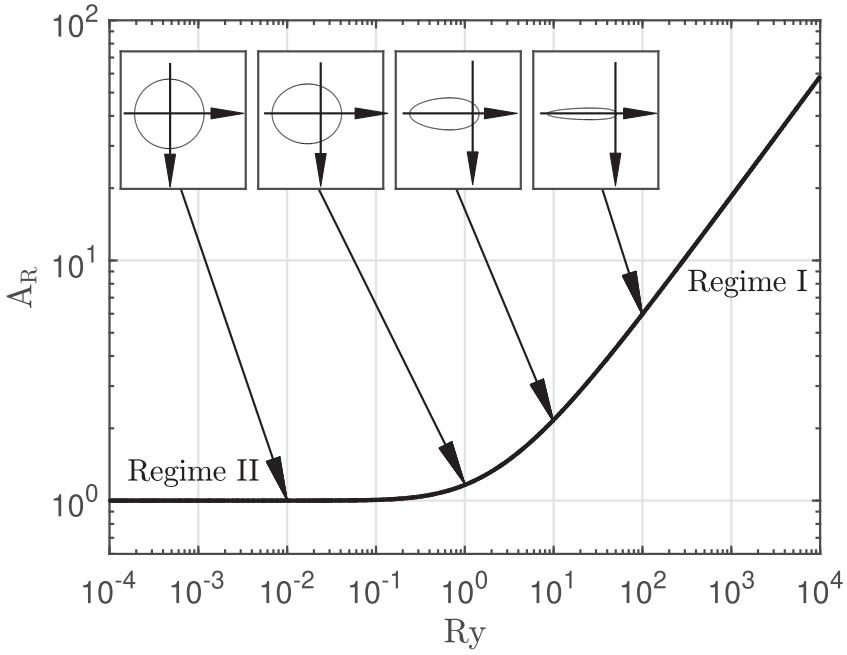

Fig. 3. Aspect ratio of the isotherm $T = T_c$ for different Ry values under a moving point heat source on a semi-infinite solid.

$$\left.\widehat{\frac{dT^*_{\max}}{dy^*}}\right|_{\mathrm{I}}(\mathrm{Ry}) = -\sqrt{2\mathrm{e}}\mathrm{Ry}^{-\frac{3}{2}} \quad \text{for Regime I (fast)} \tag{38}$$

$$\left.\widehat{\frac{dT^*_{\max}}{dy^*}}\right|_{\mathrm{II}}(\mathrm{Ry}) = -\mathrm{Ry}^{-2} \quad \text{for Regime II (slow)} \tag{39}$$

with the following correction factors

$$f_{dT_{\max}/dy|_{\mathrm{I,II}}}(\mathrm{Ry}) = \left[1 + \left(\sqrt{\frac{1}{2\mathrm{eRy}}}\right)^{\pm n}\right]^{1/n} \quad \begin{matrix} +n \text{ for Regime I (fast)} \\ -n \text{ for Regime II (slow)} \end{matrix} \tag{40}$$

The optimal value of n for Eq. (40) is $n = 3.079$, with an error always less than 6.141%. The crossover point for the correction factors is $\mathrm{Ry}_c = 0.1839$. Asymptotic expressions without correction factors result in an error smaller than 10% for $\mathrm{Ry}_{\mathrm{I}} > 0.3897$ or $\mathrm{Ry}_{\mathrm{II}} < 0.05530$ in their corresponding regimes.

The corresponding engineering expression with units can be obtained by replacing Eq. (5) into Eqs. (38) and (39), and combining with Eq. (3)

$$\begin{aligned}\widehat{\frac{dT_{\max}}{dy}}^{+} &= \left.\widehat{\frac{dT_{\max}}{dy}}\right|_{\mathrm{I}} f_{dT_{\max}/dy|_{\mathrm{I}}}(\mathrm{Ry}) \\ &= -\sqrt{\frac{2e\pi kU}{\alpha q}}(T_{\max} - T_0)^{\frac{3}{2}} f_{dT_{\max}/dy|_{\mathrm{I}}}(\mathrm{Ry}) \quad \text{for Regime I (fast)}\end{aligned} \tag{41}$$

$$\begin{aligned}\widehat{\frac{dT_{\max}}{dy}}^{+} &= \left.\widehat{\frac{dT_{\max}}{dy}}\right|_{\mathrm{II}} f_{dT_{\max}/dy|_{\mathrm{II}}}(\mathrm{Ry}) \\ &= -\frac{2\pi k}{q}(T_{\max} - T_0)^2 f_{dT_{\max}/dy|_{\mathrm{II}}}(\mathrm{Ry}) \quad \text{for Regime II (slow)}\end{aligned} \tag{42}$$

9. Aspect ratio A_R

The aspect ratio of an isotherm is a metric of how elongated the isotherm is, and because it depends only on Ry, the aspect ratio is also a proxy for Ry. In many practical applications, such as welding, key isotherms are visible; for example the melting isotherm can be observed easily, and the isotherm of 600 °C is often seen in steels as the line at which the steel starts to turn red hot; this way, a simple observation becomes a practical assessment of travel speed. Previous attempts at obtaining an explicit expression were made in [27] using a polynomial fitting over a limited range of speeds, and a linear correlation for slow speeds. The aspect ratio, A_R, is defined as the ratio of isotherm length $(x_{\mathrm{f}} - x_{\mathrm{b}})$ to isotherm width $(2y_{\max})$

$$A_R = \frac{x_{\mathrm{f}} - x_{\mathrm{b}}}{2y_{\max}} = \frac{x^*_{\mathrm{f}} - x^*_{\mathrm{b}}}{2y^*_{\max}} \tag{43}$$

Asymptotic analysis of Eq. (43) yields the following power laws for Regime I and Regime II

$$\widehat{A_{R\mathrm{I}}}(\mathrm{Ry}) = \sqrt{\frac{\mathrm{eRy}}{8}} \quad \text{for Regime I (fast)} \tag{44}$$

$$\widehat{A_{R\mathrm{II}}}(\mathrm{Ry}) = 1 \quad \text{for Regime II (slow)} \tag{45}$$

The aspect ratio of 1 in Regime II is consistent with the spherical symmetry of the pure conduction problem when there is no motion of the heat source. The correction factors using blending are the following

$$f_{A_{R\mathrm{I,II}}}(\mathrm{Ry}) = \left[1 + \left(\sqrt{\frac{8}{\mathrm{eRy}}}\right)^{\pm n}\right]^{1/n} \quad \begin{matrix} +n \text{ for Regime I (fast)} \\ -n \text{ for Regime II (slow)} \end{matrix} \tag{46}$$

The optimal value of n for Eq. (46) is $n = 1.904$, with an error always less than 1.994%. The crossover point for the correction factors is $\mathrm{Ry}_c = 2.943$. Asymptotic expressions without correction factors result in an error less than 10% for $\mathrm{Ry}_{\mathrm{I}} > 19.07$ or $\mathrm{Ry}_{\mathrm{II}} < 0.6756$ in their corresponding regimes. The corresponding engineering expression with units can be obtained by replacing Eq. (8) into Eqs. (44) and (45) to obtain

$$\widehat{A_R}^{+} = \widehat{A_{R\mathrm{I}}} f_{A_{R\mathrm{I}}}(\mathrm{Ry}) = \sqrt{\frac{eqU}{32\pi k\alpha(T_c - T_0)}} f_{A_{R\mathrm{I}}}(\mathrm{Ry}) \quad \text{for Regime I (fast)} \tag{47}$$

$$\widehat{A_R}^{+} = \widehat{A_{R\mathrm{II}}} f_{A_{R\mathrm{II}}}(\mathrm{Ry}) = f_{A_{R\mathrm{II}}}(\mathrm{Ry}) \quad \text{for Regime II (slow)} \tag{48}$$

Fig. 3 presents the aspect ratio as a function of Ry, and displays the isotherms corresponding to Ry equals to 0.01, 1, 10 and 100, showing how the isotherm becomes progressively more elongated with Ry.

10. Melting efficiency $_{\eta_m}$

Melting efficiency η_m is a magnitude defined for fusion welding processes, in which melting is essential to accomplish the joining operation. The superheat above melting is unnecessary for joining, and in the ideal case, the molten material reaches the melting point but does not exceed it, leaving the rest of the substrate unaffected. For a given cross section of a weld, a lower melting efficiency implies that more heat will affect the substrate, resulting in distortions, residual stresses, and grain coarsening. When the welding process involves a filler material, different melting efficiencies can result in different mixtures of filler and base material in the melt (dilution). Dilution is a critical factor in the welding of wear-resistant overlays [31], the welding of carbon to stainless steels [32,33] and the welding of aluminum [34]. Beyond welding, if critical temperatures other than melting are considered, the melting efficiency is an applicable parameter to other relevant thermal processes. For example, if the characteristic temperature considered is the austenitization temperature, the adapted concept of melting efficiency yields insight into the excess heat applied and potential distortions and residual stresses in laser or flame heat treating.

The melting efficiency is defined as the energy used to reach melting relative to the total energy deposited from the heat source, and it can be approximated using Rosenthal's model, acknowledging its limitations, especially the lack of proper accounting for latent heat. Despite its limitations, the conclusions obtained are qualitatively correct, and quantitatively not far from reality as shown by previous studies on melting efficiency [35–38]. Some rough corrections can be used to improve the calculations, such as using an average specific heat which includes the effect of latent heat.

For the model considered, the volumetric energy to reach melting is given by $\rho c_p(T_m - T_0)$, where ρ, c_p, and T_m are the density, specific heat, and melting temperature of the substrate respectively. The cross section of fusion zone has a cross sectional area of $\frac{\pi}{2} y_{max,m}^2$, where $y_{max,m}$ is the maximum width of the isotherm of melting temperature. The melting efficiency can then be calculated as

$$\eta_m = \frac{\rho c_p (T_m - T_0) U \frac{\pi}{2} y_{max,m}^2}{q}$$

which can be rewritten using Eqs. (8) and (5) as

$$\eta_m = \frac{1}{2} \frac{y_{max,m}^{*2}}{Ry_m} \tag{49}$$

where Ry_m correspond to T_m. Replacing the asymptotic expressions for $\hat{y}_{max}^{+}$ from [1] into Eq. (49) yields the following power laws

$$\hat{\eta}_{m_I}(Ry) = \frac{1}{e} \quad \text{for Regime I (fast)} \tag{50}$$

$$\hat{\eta}_{m_{II}}(Ry) = \frac{Ry}{2} \quad \text{for Regime II (slow)} \tag{51}$$

The blending expressions for η_m are based on those for y_{max}^{*}, resulting in

$$f_{\eta_{m_{I,II}}}(Ry) = \left[1 + \left(\frac{eRy}{2}\right)^{\pm n}\right]^{1/n} \qquad \begin{matrix} +n \text{ for Regime I (fast)} \\ -n \text{ for Regime II (slow)} \end{matrix} \tag{52}$$

The optimal value of n for Eq. (52) is $n = -0.8655$, with an error always less than 1.450%. The crossover point for the correction factors is $Ry_c = 0.7359$. Asymptotic expressions without correction factors result in an error smaller than 10% for $Ry_c > 11.85$ or $Ry_c < 0.05388$ in their corresponding regimes.

Eq. (50) indicates that for the model considered, the melting efficiency reaches a maximum value of 36.79% for very fast heat sources, but it never approaches 100%. This is a consequence of the superheat inside the molten region and the gradients on the substrate outside the molten region. Eq. (51) indicates that for slow welds, the heat lost by conduction reduces the melting efficiency significantly.

Eqs. (50) and (51) suggest that the melting efficiency is never zero, regardless of the power of the heat source; however, experience indicates that for weak heat sources sometimes there is no melting and the melting efficiency should be zero. This discrepancy is a consequence of the model being based on a point heat source reaching infinite temperature at the point of application, regardless of the power of the heat source. More sophisticated models that account for distributed heat sources such as [39] are needed to capture this phenomenon correctly, and are the focus of current research.

The corresponding engineering expressions with units can be obtained by replacing Eq. (8) into Eqs. (50) and (51), obtaining

$$\hat{\eta}_m^{+} = \hat{\eta}_{m_I} f_{\eta_{m_I}}(Ry) = \frac{1}{e} f_{\eta_{m_I}}(Ry) \quad \text{for Regime I (fast)} \tag{53}$$

$$\hat{\eta}_m^{+} = \hat{\eta}_{m_{II}} f_{\eta_{m_{II}}}(Ry) = \frac{qU}{8\pi k\alpha(T_m - T_0)} f_{\eta_{m_{II}}}(Ry) \quad \text{for Regime II (slow)} \tag{54}$$

11. Cooling time $t_{8/5}$

The characteristic value $t_{8/5}$ is typically used as a metric of cooling rate in the welding of steels, and it is defined as the time it takes for the centerline to cool from 800 °C to 500 °C. For steels, austenite decomposition occurs in this temperature range, resulting in a variety of microstructural constituents such as ferrite, pearlite, bainite, and martensite, depending on the cooling rate [40]. Similar to cooling rate $\dot{T}_b$, cooling time $t_{8/5}$ is also insensitive to the location in the vicinity of weld centerline [23,41].

For a fixed point on the centerline, the time to cool from 800 °C to 500 °C, is the time it takes for the heat source to travel the distance between the trailing length x_b of the 800 °C and 500 °C isotherms; thus

$$t_{8/5} = \frac{1}{U} \Delta x_b \Big|_{500}^{800} = \frac{q}{2\pi kU} \left(\frac{1}{T_{500} - T_0} - \frac{1}{T_{800} - T_0} \right) \tag{55}$$

The time $t_{8/5}$ can be approximated as

$$t_{8/5} \approx -\frac{1}{\dot{T}_{b,i}} \Delta T \Big|_{500}^{800} = \frac{q(T_{800} - T_{500})}{2\pi kU(T_i - T_0)^2} \tag{56}$$

where $\dot{T}_{b,i}$ is the cooling rate evaluated at a temperature T_i intermediate between 500 °C and 800 °C. This equation is equivalent to that presented in [19]. Typically, the error is small for any T_i, and it is shown in the Appendix that Eq. (56) is exact when

$$T_i - T_0 = \sqrt{(T_{800} - T_0)(T_{500} - T_0)} \qquad (T_i = 632\ ^\circ C \text{ for } T_0 = 20\ ^\circ C) \tag{57}$$

The parameters q and U appear combined and never independently in the calculation of $t_{8/5}$ Eq. (55) (and also in the determination of cooling rate). For this reason, in practice only the ratio q/U termed "linear heat input" is typically used, and embodied in codes and standards such as [42–45].

12. Solidification time at centerline t_{sl}

The model used here can be extended to capture aspects of phase transformations when their presence does not affect significantly the solution. For the case of steels in typical welding conditions, it was demonstrated in [46] that solidification and solid-state phase transformations cause only small departures from the exact solution shown in Eq. (1). To deal with phase transformations, an enthalpy-based formulation is convenient. In the original solution, the hypothesis of constant properties means that the enthalpy formulation and the temperature formulation are equivalent, and enthalpy variations can be calculated based on temperature variations. This way, in the original formulation of the problem, it is possible to state the following rate of enthalpy loss at the trailing length of the weld based on Eq. (25)

$$\left.\frac{Di}{Dt}\right|_b = -\frac{2\pi k c_p U (T_c - T_0)^2}{q} \qquad \text{Regime I (fast) and II (slow)} \tag{58}$$

where i is enthalpy per unit mass, and c_p is the effective specific heat considered constant in Rosenthal's formulation, and for this reason is not necessary to attribute it to solid or liquid. Because phase transformations have a small effect on the solution, this rate of enthalpy loss can be used to estimate the time associated with the dissipation of enthalpy from a phase transformation. For the case of solidification, the latent heat of solidification i_{sl} would take a time t_{sl} to be dissipated, which can be estimated as

$$t_{sl} = -\frac{i_{sl}}{Di/Dt|_b} = \frac{q i_{sl}}{2\pi k c_p U (T_m - T_0)^2} \qquad \text{Regime I (fast) and II (slow)} \tag{59}$$

where T_m ("melting temperature") is a temperature representative of the solidification. Because of the approximate nature of the calculation, it is not possible to give an exact number; however, solidification typically happens over a relatively narrow range of temperatures, and for practical calculations it can be considered that T_m is an intermediate between the liquidus and solidus temperature of the alloy in question. Eq. (59) has also been presented in [47,48] and has been applied in [49,50] to study nonequilibrium solidification conditions. The dimensionless counterpart of Eq. (59) is

$$t^*_{sl} = \frac{\mathrm{Ry}}{\mathrm{St}} \qquad \text{Regime I (fast) and II (slow)} \tag{60}$$

where time is normalized according to Eq. (22), Ry is considered at T_m, and St is the Stefan number

$$\mathrm{St} = \frac{c_p (T_m - T_0)}{i_{sl}} \tag{61}$$

For typical structural steel, the Stefan number is approximately 3 [51]. The analysis above can be extended to other phase transformations such as austenite decomposition, and Eq. (58) could be the basis to extend the calorimetry analysis of phase transformations of [52,53] to in situ analysis of transformations in welding and surface heat treating.

13. Thickness of the heat affected zone y_{HAZ}

The heat affected zone (HAZ) is an extremely important concept in welding and thermal cutting of all metals, and it is defined as the layer of material surrounding the fusion line that is affected by the heat. In steels, it typically corresponds to the material that was exposed to temperatures between slightly below the beginning of austenitization ($A_{c,1}$) and melting (T_m) [40]. The microstructures in the HAZ are typically undesirable, and a narrower HAZ can often enable welds that would not have been performed acceptably otherwise.

Mathematically, the thickness of the heat affected zone can be defined as

$$\Delta y_{HAZ} = y_{HAZ,m} - y_{max,m} \tag{62}$$

where $y_{max,HAZ}$ is the width of the isotherm T_{HAZ} that marks the edge of the HAZ; for example $A_{c,1}$ in steels, and $y_{max,m}$ is the width of the melting isotherm (T_m, marking the width of the weld). Substituting T_{HAZ} and T_m into Eqs. (11) and (12) results in the following predictions for thickness of the HAZ

$$\Delta y_{HAZ} = \sqrt{\frac{2\alpha q}{\pi e k U}}\left[\frac{f_{y_{max_I}}(\mathrm{Ry}_{T_{HAZ}})}{\sqrt{T_{HAZ} - T_0}} - \frac{f_{y_{max_I}}(\mathrm{Ry}_{T_m})}{\sqrt{T_m - T_0}}\right] \quad \text{for Regime I (fast)} \tag{63}$$

$$\Delta y_{HAZ} = \frac{q}{2\pi k}\left[\frac{f_{y_{max_{II}}}(\mathrm{Ry}_{T_{HAZ}})}{T_{HAZ} - T_0} - \frac{f_{y_{max_{II}}}(\mathrm{Ry}_{T_m})}{T_m - T_0}\right] \quad \text{for Regime II (slow)} \tag{64}$$

For a relatively thin HAZ, its thickness approximated also as

$$\Delta y_{HAZ} \approx -\frac{1}{dT_{max}/dy|_i}\Delta T\Big|_{T_{HAZ}}^{T_m} = \sqrt{\frac{q\alpha}{2e\pi k U}}\frac{T_m - T_{HAZ}}{(T_i - T_0)^{\frac{3}{2}}} \quad \text{for Regime I (fast)} \tag{65}$$

$$\Delta y_{HAZ} \approx -\frac{1}{dT_{max}/dy|_i}\Delta T\Big|_{T_{HAZ}}^{T_m} = \frac{q(T_m - T_{HAZ})}{2\pi k (T_i - T_0)^2} \quad \text{for Regime II (slow)} \tag{66}$$

where $dT_{max}/dy|_i$ is the gradient of maximum temperature in a cross section evaluated at a temperature T_i intermediate between T_{HAZ} and T_m. Typically, the error is small for any T_i, and using the expression derived in the Appendix, Eqs. (65) and (66) is exact when

$$T_i - T_0 = \left[\sqrt{(T_{HAZ} - T_0)(T_m - T_0)}\frac{\sqrt{T_{HAZ} - T_0} + \sqrt{T_m - T_0}}{2}\right]^{2/3} \quad \text{for Regime I (fast)} \tag{67}$$

$$T_i - T_0 = \sqrt{(T_{HAZ} - T_0)(T_m - T_0)} \quad \text{for Regime II (slow)} \tag{68}$$

Typical values for plain carbon steel are $T_{HAZ} \approx 750\,^\circ\mathrm{C}$ and $T_m \approx 1500\,^\circ\mathrm{C}$, and for a starting temperature $T_0 = 20\,^\circ\mathrm{C}$, this results in $T_i = 1070\,^\circ\mathrm{C}$ for Regime I, and a very similar $T_i = 1059\,^\circ\mathrm{C}$ for Regime II (11 °C apart). In comparison, the arithmetic mean of temperatures results in $T_i = (T_{HAZ} + T_m)/2 = 1125\,^\circ\mathrm{C}$ (55 °C and 66 °C above the exact intermediate temperatures). Given the simplicity of calculation of intermediate temperature for Regime II, and how it also represents the intermediate temperature in Regime I much closer than the arithmetic mean, it is practical (and typically accurate) to use Eq. (68) for all values of Ry when estimating an intermediate temperature when using a temperature gradient to estimate the width of the HAZ.

14. Effect of joint preparation geometry

Eq. (1) has symmetry of revolution around the x-axis. The implication of this symmetry is that the problem formulation is the same for other configurations with symmetry of revolution such as a full solid, or a wedge of angle ϕ with its edge along the x-axis (which is a good representation of a beveled weld joint preparation in a thick plate). All problems with the same "angular heat intensity" defined as q/ϕ will have the same solution; for the case of a semi-infinite solid, $\phi = 180^\circ$. The formulae presented above for a semi-infinite solid can be applied without additional mathematical error to the other related problems replacing the heat intensity q with an "effective heat intensity" q_{eff} that accounts for the different angle covered in the cylindrical symmetry.

$$q_{eff} = \frac{180^\circ}{\phi} q \tag{69}$$

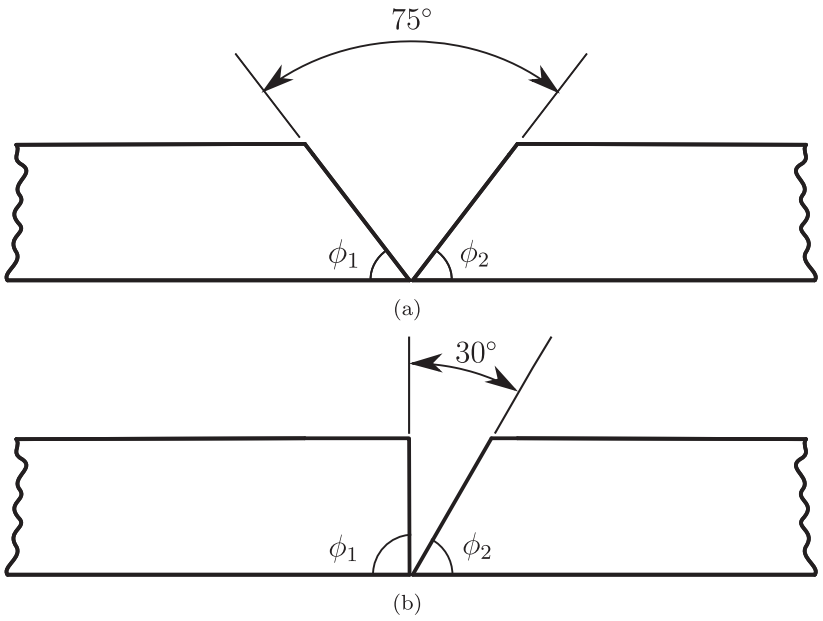

Fig. 4. Schematic of V-groove joint preparation (a), and single bevel joint preparation (b).

where ϕ is in degrees. A particular practical application of this extended analysis is weld joint preparations, for which the analysis is valid as long as the isotherm of interest (T_c) is well inside the beveled edges, and far from the edge where the bevel meets the top surface of the plate. For example, for the 75° V-groove joint preparation shown in Fig. 4a, assuming that the heat is divided evenly between the two halves of the joint preparation, all formulae derived above are applicable when q is replaced by $q_{\text{eff}} = (q/2) \times (180^\circ/52.5^\circ) = 1.714q$. The division by 2 is because only half of the heat goes to each plate, and the 52.5° correspond to the angle covered by the solid for each plate (52.5° = 90°-75°/2). Predicted cooling time from 800 °C to 500 °C, $t_{8/5}$, and cooling rate $\dot{T}_b$ at 650 °C in root pass welding of steel plates with the groove joint preparation are in agreement with general experience [54].

For the case in which the two sides of a joint have different preparation, such as the single bevel groove joint of Fig. 4b, the distribution of heat is typically not even between the two sides. If the same characteristic values (e.g. cooling rate or width of melting isotherm) are desirable for both sides of the joint, the effective heat intensity should be the same on both sides, resulting in a distribution of heat proportional to the wedge angle of each side

$$\frac{q_j}{q} = \frac{\phi_j}{\phi_1 + \phi_2} \tag{70}$$

where $j = 1, 2$ identifies each side of the joint, such that q_1 and q_2 are the amounts of heat on each side of the joint, and ϕ_1 and ϕ_2 are their corresponding wedge angles. For example, for the 30° single bevel of Fig. 4b, $\phi_1 = 90^\circ$ for the square side, and $\phi_2 = 60^\circ$ for the beveled side, resulting in $q_1 = 0.6q$ and $q_2 = 0.4q$. In this case, if similar properties are desired for both sides of the joint, the partition of heat for welding should be 60% on the square side, and 40% on the beveled side. This partition is typically accomplished in practice by making an asymmetric weave and/or having different dwell times on each side during the weave. The width of the weave is small, of the order of the width of the molten metal, and a weaved weld is typically considered a straight line in practice. Eq. (70) can be of much help in anticipating the different dwell times needed.

15. Discussion

The results presented here are novel, with the main difference with previous attempts is the use of blending techniques to provide explicit solutions for the entire range of parameters; this had never been accomplished before. Another important difference is the identification of a single dimensionless group determines all characteristic values (instead of two as in [55]). This dimensionless group is typically the Rykalin number, which had been proposed before [37] based on the analysis of experiments, but had not been adopted by the community.

The expressions developed are based on fundamental principles, are simple and general, and are within 7% of the exact solution. Such combination is desirable, and uncommon. For values of Ry larger than 20 or smaller than 1/20, the correction factors account for less than 10% and can be omitted; in these cases, the final expressions are even simpler. Many practical applications, such as heat sources based on lasers and electron beams are consistently at Ry much larger than 20. The mathematical analysis is proven in detail in this work; however, the next obvious question is whether the exact solution (Eq. (1)) is close enough to reality for the expressions presented to be of practical use.

The accuracy of the exact solution has been validated through intensive testing [56,55,57–61] and numerical analysis [46,62–64]. The effect of variable materials properties and latent heat was analyzed numerically in [46], where it was shown that these effects resulted in variations below 10% in the trailing length.

Christensen's work [55] was especially thorough, and validated the exact solution for the case of welding using many characteristic values in common with those presented here (experiments tested $y_{\max}$ both as width and depth, $x_{\max}, x_f - x_b, x_{\max} - x_b, T_{\max}, \dot{T}_b$). The validation considered multiple welding processes and materials. The reference temperature considered was the melting temperature, which is beyond the range of validity of the model, and the results were still consistent with the model. The predictions for width, trailing length, and cooling rate are typically useful for engineering purposes, while the predictions for leading length for the melting temperature tend to be underestimates, because the size of the heat source is typically larger than the leading length.

Table 1
Summary of characteristic values and correction factors.

Variable	Regime	Asymptotic	Correction factor	n	Error [%]	Eq.
y_{max}	I	$\sqrt{\frac{2}{\pi e}\frac{\alpha q}{kU(T_c-T_0)}}$	$\left[1+\left(\sqrt{\frac{eRy}{2}}\right)^n\right]^{\frac{1}{n}}$	−1.73	0.7	(11)
	II	$\frac{1}{2\pi}\frac{q}{k(T_c-T_0)}$	$\left[1+\left(\sqrt{\frac{eRy}{2}}\right)^{-n}\right]^{\frac{1}{n}}$			(12)
x_{max}	I	$-\frac{q}{2\pi ek(T_c-T_0)}$	$\left[1+(eRy)^n\right]^{\frac{1}{n}}$	−1.00	1.9	(16)
	II	$-\frac{2U}{\alpha}\left[\frac{q}{4\pi k(T_c-T_0)}\right]^2$	$\left[1+(eRy)^{-n}\right]^{\frac{1}{n}}$			(17)
x_b	I and II	$-\frac{q}{2\pi k(T_c-T_0)}$				(20)
$\dot{T}_b$	I and II	$-\frac{2\pi kU(T_c-T_0)^2}{q}$				(25)
x_f	I and II	$\frac{\alpha}{U}W_0\left[\frac{qU}{2\pi k\alpha(T_c-T_0)}\right]$				(29)
$\dot{T}_f$	I and II	$\frac{U^2(T_c-T_0)}{\alpha}\left[\frac{1}{W_0(2Ry)}+1\right]$				(31)
T_{max}	I	$T_0+\frac{2\alpha q}{e\pi kUy_c^2}$	$\left[1+\left(\frac{eUy_c}{4\alpha}\right)^n\right]^{\frac{1}{n}}$	−1.25	3.9	(35)
	II	$T_0+\frac{q}{2\pi ky_c}$	$\left[1+\left(\frac{eUy_c}{4\alpha}\right)^{-n}\right]^{\frac{1}{n}}$			(36)
dT_{max}/dy	I	$-\sqrt{\frac{2e\pi kU}{q\alpha}}(T_m-T_0)^{\frac{3}{2}}$	$\left[1+\left(\sqrt{\frac{1}{2eRy}}\right)^n\right]^{\frac{1}{n}}$	3.08	6.1	(41)
	II	$-\frac{2\pi k}{q}(T_m-T_0)^2$	$\left[1+\left(\sqrt{\frac{1}{2eRy}}\right)^{-n}\right]^{\frac{1}{n}}$			(42)
A_R	I	$\sqrt{\frac{eqU}{32\pi k\alpha(T-T_0)}}$	$\left[1+\left(\sqrt{\frac{8}{eRy}}\right)^n\right]^{\frac{1}{n}}$	1.90	2.0	(47)
	II	1	$\left[1+\left(\sqrt{\frac{8}{eRy}}\right)^{-n}\right]^{\frac{1}{n}}$			(48)
η_m	I	$\frac{1}{e}$	$\left[1+\left(\frac{eRy}{2}\right)^n\right]^{\frac{1}{n}}$	−0.87	1.4	(53)
	II	$\frac{qU}{8\pi k\alpha(T_m-T_0)}$	$\left[1+\left(\frac{eRy}{2}\right)^{-n}\right]^{\frac{1}{n}}$			(54)
$t_{8/5}$	N/A	$\frac{q}{2\pi kU}\left(\frac{1}{T_{500}-T_0}-\frac{1}{T_{800}-T_0}\right)$				(55)
$t_{8/5}$	N/A	$t_{8/5}\approx\frac{q(T_{800}-T_{500})}{2\pi kU(T_i-T_0)^2}$				(56)
		$T_i-T_0=\sqrt{(T_{800}-T_0)(T_{500}-T_0)}$			*	(57)
t_{sl}	N/A	$\frac{qi_{sl}}{2\pi kc_pU(T_m-T_0)^2}$				(59)
Δy_{HAZ}	I	$\sqrt{\frac{2\alpha q}{\pi ekU}}\left[\frac{f_{ymax_I}(Ry_{T_{HAZ}})}{\sqrt{T_{HAZ}-T_0}}-\frac{f_{ymax_I}(Ry_{T_m})}{\sqrt{T_m-T_0}}\right]$	$\left[1+\left(\sqrt{\frac{eRy}{2}}\right)^n\right]^{\frac{1}{n}}$	−1.73	0.7	(63)
	II	$\frac{q}{2\pi k}\left[\frac{f_{ymax_{II}}(Ry_{T_{HAZ}})}{T_{HAZ}-T_0}-\frac{f_{ymax_{II}}(Ry_{T_m})}{T_m-T_0}\right]$	$\left[1+\left(\sqrt{\frac{eRy}{2}}\right)^{-n}\right]^{\frac{1}{n}}$			(64)
Δy_{HAZ}	I	$\Delta y_{HAZ}\approx\sqrt{\frac{q\alpha}{2e\pi kU}}\frac{T_m-T_{HAZ}}{(T_i-T_0)^{\frac{3}{2}}}$	$\left[1+\left(\sqrt{\frac{1}{2eRy}}\right)^n\right]^{-\frac{1}{n}}$	3.08	6.1	(65)
		$T_i-T_0=\left[\sqrt{(T_{HAZ}-T_0)(T_m-T_0)}\frac{\sqrt{T_{HAZ}-T_0}+\sqrt{T_m-T_0}}{2}\right]^{2/3}$			*	(67)
	II	$\Delta y_{HAZ}\approx\frac{q(T_m-T_{HAZ})}{2\pi k(T_i-T_0)^2}$	$\left[1+\left(\sqrt{\frac{1}{2eRy}}\right)^{-n}\right]^{-\frac{1}{n}}$	3.08	6.1	(66)
		$T_i-T_0=\sqrt{(T_{HAZ}-T_0)(T_m-T_0)}$			*	(68)

* Using these intermediate temperatures the calculation using the derivative is exactly the same as that using differences.

Estimate of weld penetration is also typically unreliable because convection in the molten metal plays a significant role. It is remarkable that Rosenthal's idealized solution was proved to be effective despite of its simplicity.

The accuracy of the expressions presented here is affected in practice by the limitations of the exact solution. Some of this limitations can be overcome in practical ways. The limitation of constant thermophysical properties can be addressed in a practical way by using effective values, such as those proposed in [5]. The limitation of a point heat source can be addressed with the consideration of distributed heat sources, which would add precision and physical meaning with as little as a single extra parameter (dimensionless size of the heat source). The limitation of considering only conduction can be addressed by accounting for the effect of fluid flow as in [65], which would add two dimensionless groups (Prandtl number and Marangoni number). The consideration of infinite thickness of the substrate can be addressed by blending with the 2D solutions for moving heat sources (often called the "thin plate solution"). The challenge in this case is that blending must be extended to asymptotic behaviors beyond power laws and to two or more dimensionless groups. Blending under these conditions is beyond the capabilities of [6,7]. These challenges are the current focus of intense research. The 2D solutions are also the common approach for the welding and cutting cases in which there is a keyhole [66,67,11], and is also the focus of current work outside the scope of this paper.

The ultimate goal of the estimates and correction factors presented here is to serve as accurate predictors of actual processes, in a similar way that moving heat source equations from [17] are used in [68]. In these references, the asymptotic solutions are modified with empirical correction factors. These empirical modifications are not based on fundamental analysis, resulting in two important drawbacks: first, these modifications are valid only for the materials and processes used in the calibrations, and second, the range of parameters for which these calibrations are valid is not clearly defined.

16. Conclusions

Equations for characteristic values are listed in Table 1, including maximum isotherm width and its location, leading and trailing lengths of the isotherm, centerline heating and cooling rates, maximum temperature and its gradient, aspect ratio of isotherm, cooling time $t_{8/5}$, solidification time, thickness of the affected zone, and modification coefficient for joint preparation geometry.

For Ry $<$ 1/20 or Ry $>$ 20, the asymptotic solutions alone (without correction factor) yield an error below 10% when compared to the exact solution for all listed characteristic values. As a general rule of thumb, a moving heat source can be considered "slow" when Ry $<$ 1/20 and "fast" when Ry $>$ 20.

Key characteristics of isotherms produced by a given set of experimental parameters can be calculated with ubiquitous means such as scientific calculators or spreadsheets. In addition to predictive estimations, the engineering expressions also enhance intuition and reflect quantitative effects of different process parameters and their combination on resulting thermal conditions. The methodology and engineering expressions obtained can be applied into a number of processes and materials in different disciplines since they capture the inherent essence of complex physical phenomena based on fundamental physics.

Conflict of Interest

The authors declared that there is no conflict of interest.

Acknowledgment

The authors wish to acknowledge funding support from the Natural Sciences and Engineering Research Council of Canada (NSERC), and the China Scholarship Council (CSC). Student scholarships from the American Welding Society and the Canadian Welding Association Foundation were gratefully received.

Appendix A. Relationship between the derivatives and variations in power-law asymptotic regimes

Consider a problem in which the characteristic values depend on a single dimensionless group Π (in this paper, the single dimensionless group is typically Ry). Consider also two characteristic values with power-law dependence on Π

$$u_c(\Pi) = A\Pi^m \tag{.1}$$

$$v_c(\Pi) = B\Pi^n \tag{.2}$$

There is an intermediate value of Π for which the following calculation is exact

$$\left.\frac{du_c}{dv_c}\right|_{\Pi_i} = \frac{u_c(\Pi_2) - u_c(\Pi_1)}{v_c(\Pi_2) - v_c(\Pi_1)} \tag{.3}$$

where Π_1 and Π_2 are two separate values and Π_i is the intermediate value sought. To calculate the value of Π_i where Eq. (.3) is exact, we can analyze the derivative and the ratio of variations

$$\left.\frac{du_c}{dv_c}\right|_{\Pi_i} = \left.\frac{du_c/d\Pi}{dv_c/d\Pi}\right|_{\Pi_i} = \frac{A}{B}\frac{m}{n}\Pi_i^{m-n} \tag{.4}$$

$$\frac{\Delta u_c}{\Delta v_c} = \frac{A}{B}\frac{\Pi_2^m - \Pi_1^m}{\Pi_2^n - \Pi_1^n} \tag{.5}$$

Combining Eqs. (.3), (.4) and (.5) results in the following value for Π_i, for which the derivative and the ratio of variations give exactly the same result

$$\Pi_i = \left(\frac{n}{m}\frac{\Pi_2^m - \Pi_1^m}{\Pi_2^n - \Pi_1^n}\right)^{\frac{1}{m-n}} \tag{.6}$$

This expression is exact only for power-law asymptotic regimes, but it is still a useful approximation for intermediate regimes. As an example of application of Eq. (.6), consider the case of cooling rate and $t_{8/5}$, where $\Pi = \mathrm{Ry}, u_c = T_b^*$, and $v_c = x_b^*$. From Eq. (3), we obtain $m = -1$, from Eq. (19), $n = 1$, resulting in

$$\mathrm{Ry}_i = \left(-\frac{\mathrm{Ry}_2^{-1} - \mathrm{Ry}_1^{-1}}{\mathrm{Ry}_2 - \mathrm{Ry}_1}\right)^{\frac{1}{-1-1}} = \sqrt{\mathrm{Ry}_1\mathrm{Ry}_2} \tag{.7}$$

which becomes Eq. (57) when the definition of Ry is used.

References

[1] P.F. Mendez, Y. Lu, Y. Wang, Scaling analysis of a moving point heat source in steady-state on a semi-infinite solid, J. Heat Transfer 140 (2018) 081301.
[2] H.A. Wilson, On convection of heat, Proc. Cambridge Philosoph. Soc. 12 (1904) 406–423.
[3] O.F.T. Roberts, The theoretical scattering of smoke in a turbulent atmosphere, Proc. Roy. Soc. London. Series A, Contain. Papers Mathe. Phys. Charact. 104 (728) (1923) 640–654.
[4] D. Rosenthal, The theory of moving sources of heat and its application to metal treatments, Trans. ASME 68 (1946) 849–866.
[5] P.W. Fuerschbach, G.R. Eisler, Determination of material properties for welding models by means of Arc weld experiments, in: 6th Intl. Trends in Welding Research, Pine Mountain, Georgia, 2002, pp. 782–786.
[6] S.W. Churchill, R. Usagi, A general expression for the correlation of rates of transfer and other phenomena, AIChE J. 18 (6) (1972) 1121–1128.
[7] S.W. Churchill, R. Usagi, A standardized procedure for the production of correlations in the form of a common empirical equation, Ind. Eng. Chem. Fund. 13 (1) (1974) 39–44.
[8] Y.S. Muzychka, M.M. Yovanovich, Thermal resistance models for non-circular moving heat sources on a half space, J. Heat Transfer 123 (4) (2001) 624–632.
[9] A. Acrivos, A rapid method for estimating the shear stress and the separation point in laminar incompressible boundary-layer flows, J. Aero/Space Sci. 27 (4) (1960) 314–315.
[10] A. Acrivos, On the solution of the convection equation in laminar boundary layer flows, Chem. Eng. Sci. 17 (6) (1962) 457–465.
[11] K. Heller, S. Kessler, F. Dorsch, P. Berger, T. Graf, Analytical description of the surface temperature for the characterization of laser welding processes, Int. J. Heat Mass Transf. 106 (2017) 958–969.
[12] W. Liu, J.N. DuPont, Effects of melt-pool geometry on crystal growth and microstructure development in laser surface-melted superalloy single crystals. mathematical modeling of single-crystal growth in a melt pool (Part I), Acta Mater. 52 (16) (2004) 4833–4847.
[13] J.W. Elmer, W.H. Giedt, T.W. Eagar, The transition from shallow to deep penetration during electron beam welding, Weld. J. Res. Suppl. 69 (5) (1990) 167s–176s.
[14] E. Soylemez, J.L. Beuth, K. Taminger, Controlling melt pool dimensions over a wide range of material deposition rates in electron beam additive manufacturing, in: Proceedings of 21st Solid Freeform Fabrication Symposium, Austin, TX, 2010, pp. 571–582.
[15] W.F. Hess, L.L. Merrill, E.F. Nippes, A.P. Bunk, The measurement of cooling rates associated with Arc welding and their application to the selection of optimum welding conditions, Weld. J. 22 (9) (1943) 377–422.
[16] C.M. Adams, Cooling rates and peak temperatures in fusion welding, Weld. J. 37 (5) (1958) 210–215.
[17] M. Inagaki, H. Nakamura, A. Okada, Studies of cooling processes in the cases of welding with coated electrode and submerged Arc welding, J. Japan Weld. Soc. 34 (10) (1965) 1064–1075.
[18] B.A. Graville, Weld cooling rates and heat-affected zone hardness in a carbon steel, Weld. J. Res. Suppl. 52 (9) (1973) 377s–385s.
[19] D. Rosenthal, Mathematical theory of heat distribution during welding and cutting, Weld. J. 20 (5) (1941) 220–234.
[20] M.L. Greeff, M.D. Toit, Looking at the sensitization of 11-12 % chromium EN 1.4003 stainless steels during welding, Weld. J. 85 (11) (2006) 243s–251s.
[21] W. Hofmeister, M. Griffith, M. Ensz, J. Smugeresky, Solidification in direct metal deposition by LENS processing, J. Min., Metals Mater. Soc. 53 (9) (2001) 30–34.
[22] J.C. Ion, Laser Processing of Engineering Materials: Principles, Procedure and Industrial Application, Elsevier, Butterworth-Heinemann, Oxford, 2005.
[23] M. Inagaki, Welding conditions of steels and cooling time near the fusion line (report 1), J. Japan Weld. Soc. 27 (12) (1958) 716–722.
[24] H.K.D.H. Bhadeshia, L.E. Svensson, B. Gretoft, A model for the development of microstructure in low-alloy steel (Fe-Mn-Si-C) weld deposits, Acta Metall. 33 (7) (1985) 1271–1283.
[25] L.E. Svensson, B. Gretoft, H.K.D.H. Bhadeshia, An analysis of cooling curves from the fusion zone of steel weld deposits, Scand. J. Metall. 15 (97) (1986) 97–103.
[26] K. Poorhaydari, B. Patchett, D.G. Ivey, Estimation of cooling rate in the welding of plates with intermediate thickness, Weld. J. 84 (10) (2005) 149s–155s.

[27] A.J. Pinkerton, L. Li, Modelling the geometry of a moving laser melt pool and deposition track via energy and mass balances, J. Phys. D: Appl. Phys. 37 (14) (2004) 1885–1895.
[28] P. Peyre, P. Aubry, R. Fabbro, R. Neveu, A. Longuet, Analytical and numerical modelling of the direct metal deposition laser process, J. Phys. D: Appl. Phys. 41 (2) (2008) 025403.
[29] R.M. Corless, G.H. Gonnet, D.E.G. Hare, D.J. Jeffrey, D.E. Knuth, On the lambert W function, Adv. Comput. Mathe. 5 (1) (1996) 329–359.
[30] D.A. Barry, J. Parlange, L. Li, H. Prommer, C.J. Cunningham, F. Stagnitti, Analytical approximations for real values of the lambert W-function, Mathe. Comput. Simul. 53 (2000) 95–103.
[31] S.D. Borle, I. Le Gall, P.F. Mendez, Primary chromium carbide fraction control with variable polarity SAW, Weld. J. 94 (January) (2015) 1–7.
[32] E.J. Barnhouse, J.C. Lippold, Microstructure/property relationships in dissimilar welds between duplex stainless steels and carbon steels, Weld. J. Res. Suppl. 77 (12) (1998) 477s–487s.
[33] A. Bahrami, D.K. Aidun, Modeling of carbon steel-duplex stainless steel GTA weld pool, Weld. J. 93 (7) (2014) 262s–270s.
[34] N. Coniglio, C. Cross, T. Michael, M. Lammers, Defining a critical weld dilution to avoid solidification cracking in aluminum, Weld. J. 87 (8) (2008) 237s–247s.
[35] R.W. Niles, C.E. Jackson, Weld thermal efficiency of the GTAW process, Weld. J. 54 (1) (1975) 25–32.
[36] A. Okada, Application of melting efficiency welding and its problems, J. Japan Weld. Soc. 46 (2) (1977) 53–61.
[37] P.W. Fuerschbach, G. Knorovsky, A study of melting efficiency in plasma Arc and gas tungsten Arc welding, Weld. J. 70 (11) (1991) 287–297.
[38] J.N. DuPont, A.R. Marder, Thermal efficiency of Arc welding processes, Weld. J.-Includ. Weld. Res. Suppl. 74 (12) (1995) 406s–416s.
[39] T.W. Eagar, N.S. Tsai, Temperature fields produced by traveling distributed heat sources, Weld. J. 62 (12) (1983) 346–355.
[40] S. Kou, Welding Metallurgy, 2nd ed., John Wiley & Sons, Inc., Hoboken, New Jersey, 2003.
[41] T. Kasuya, N. Yurioka, Prediction of welding thermal history by a comprehensive solution, Weld. J. 72 (3) (1993) 107–115.
[42] ASME Section IX: Boiler and Pressure Vessel Code, Qualification Standard for Welding and Brazing Procedures, Welders, Brazers, and Welding and Brazing Operators, American Society of Mechanical Engineers, New York, 2010.
[43] BS EN 1011-2:2001, Welding–Recommendations for Welding of Metallic Materials–Part 2: Arc Welding of Ferritic Steels, British Standards Institution, London, 2001.
[44] AWS D1.1/D1.1M:2015, Structural Welding Code–Steel, American Welding Society, the United States of America, 2015.
[45] CSA W59-13, Welded Steel Construction (Metal Arc Welding), Canadian Standards Association, Canada, 2013.
[46] M. Ushio, T. Ishimura, F. Matsuda, Y. Arata, Theoretical calculation on shape of fusion boundary and temperature distribution around moving heat source (report I), Trans. JWRI 6 (1) (1977) 1–6.
[47] R.W. Messler Jr., Principles of Welding: Processes, Physics, Chemistry, and Metallurgy, John Wiley & Sons, New York, 2004.
[48] T.J. Lienert, S.S. Badu, T.A. Siewert, V.L. Acoff, ASM handbook, Welding Fundamentals and Processes, vol. 06A, ASM International, Materials Park, Ohio, 2011.
[49] J.N. DuPont, Solidification of an alloy 625 weld overlay, Metall. Mater. Trans. A 27A (11) (1996) 3612–3620.
[50] F.F. Noecker II, J.N. DuPont, Microstructural development and solidification cracking susceptibility of Cu deposits on steel: part I, J. Mater. Sci. 42 (2) (2007) 495–509.
[51] J. Miettinen, Calculation of solidification-related thermophysical properties for steels, Metall. Mater. Trans. B 28 (2) (1997) 281–297.
[52] J.W. Gibbs, C. Schlacher, A. Kamyabi-Gol, P. Mayr, P.F. Mendez, Cooling curve analysis as an alternative to dilatometry in continuous cooling transformations, Metall. Mater. Trans. A 46A (1) (2015) 148–155.
[53] A. Kamyabi-Gol, P.F. Mendez, The evolution of the fraction of individual phases during a simultaneous multiphase transformation from time – temperature data, Metall. Mater. Trans. A 46 (2) (2015) 622–638.
[54] O.M. Akselsen, G. Sagmo, Technical Report STF34 A89147, Tech. Rep., Sintef-Division of Metallurgy, Trondheim (Norway), 1989.
[55] N. Christensen, V.D.L. Davies, K. Gjermundsen, Distribution of temperatures in Arc welding, British Weld. J. (1965) 54–75.
[56] N.N. Rykalin, Calculation of Heat Flow in Welding, Mashgis, Moscow, 1951.
[57] P.S. Myers, O.A. Uyehara, G.L. Borman, Fundamentals of Heat Flow in Welding, Welding Research Council, New York, 1967.
[58] O.R. Myhr, Ø. Grong, Dimensionless maps for heat flow analyses in fusion welding, Acta Metall. Et Mater. 38 (3) (1990) 449–460.
[59] O.R. Myhr, Ø. Grong, Process modelling applied to 6082-T6 aluminium weldments–II. Applications of model, Acta Metall. Mater. 39 (11) (1991) 2703–2708.
[60] N.T. Nguyen, A. Ohta, K. Matsuoka, N. Suzuki, Y. Maeda, Analytical solutions for transient temperature of semi-infinite body subjected to 3-D moving heat sources, Weld. J. Res. Suppl. 78 (August) (1999) 265s–274s.
[61] D. Grewell, A. Benatar, Modeling heat flow for a moving heat source to describe scan micro-laser welding, in: ANTEC, 2003, pp. 1045–1050.
[62] Y. Wang, J. Lin, Characterization of the laser cleaving on glass sheets with a line-shape laser beam, Opt. Laser Technol. 39 (5) (2007) 892–899.
[63] W. Perret, C. Schwenk, M. Rethmeier, Comparison of analytical and numerical welding temperature field calculation, Comput. Mater. Sci. 47 (4) (2010) 1005–1015.
[64] D. Darmadi, J. Norrish, A.K. Tieu, Analytic and finite element solutions for temperature profiles in welding using varied heat source models, World Acad. Sci., Eng. Technol. 81 (2011) 154–162.
[65] D. Rivas, S. Ostrach, Scaling of low-Prandtl-Number thermocapillary flows, Int. J. Heat Mass Transf. 35 (6) (1992) 1469–1479.
[66] D.T. Swift-Hook, A.E.F. Gick, Penetration welding with lasers, Weld. J. Res. Suppl. 52 (11) (1973) 492s–499s.
[67] W. Steen, J. Dowden, M. Davis, P. Kapadia, A point and line source model of laser keyhole welding, J. Phys. D: Appl. Phys. 21 (8) (1988) 1255.
[68] P. Seyffarth, B. Meyer, A. Scharff, Grosser Atlas Schweiss-ZTU-Schaubilder, Fachbuchreihe Schweisstechnik, Deutscher Verlag für Schweisstechnik, Düsseldorf, 1992.